



AFRL-RX-WP-TP-2008-4336

**DEFECT OCCURRENCE AND MODELING FOR THE
THERMOMECHANICAL PROCESSING OF AEROSPACE
ALLOYS (PREPRINT)**

S.L. Semiatin, P.D. Nicolaou, J.P. Thomas, and T.J. Turner

Metals Branch

Metals, Ceramics, and NDE Division

JULY 2007

Approved for public release; distribution unlimited.

See additional restrictions described on inside pages

STINFO COPY

**AIR FORCE RESEARCH LABORATORY
MATERIALS AND MANUFACTURING DIRECTORATE
WRIGHT-PATTERSON AIR FORCE BASE, OH 45433-7750
AIR FORCE MATERIEL COMMAND
UNITED STATES AIR FORCE**

REPORT DOCUMENTATION PAGE				<i>Form Approved</i> OMB No. 0704-0188	
<small>The public reporting burden for this collection of information is estimated to average 1 hour per response, including the time for reviewing instructions, searching existing data sources, gathering and maintaining the data needed, and completing and reviewing the collection of information. Send comments regarding this burden estimate or any other aspect of this collection of information, including suggestions for reducing this burden, to Department of Defense, Washington Headquarters Services, Directorate for Information Operations and Reports (0704-0188), 1215 Jefferson Davis Highway, Suite 1204, Arlington, VA 22202-4302. Respondents should be aware that notwithstanding any other provision of law, no person shall be subject to any penalty for failing to comply with a collection of information if it does not display a currently valid OMB control number. PLEASE DO NOT RETURN YOUR FORM TO THE ABOVE ADDRESS.</small>					
1. REPORT DATE (DD-MM-YY) July 2007		2. REPORT TYPE Journal Article Preprint		3. DATES COVERED (From - To)	
4. TITLE AND SUBTITLE DEFECT OCCURRENCE AND MODELING FOR THE THERMOMECHANICAL PROCESSING OF AEROSPACE ALLOYS (PREPRINT)				5a. CONTRACT NUMBER In-house	
				5b. GRANT NUMBER	
				5c. PROGRAM ELEMENT NUMBER 62102F	
6. AUTHOR(S) S.L. Semiatin and T.J. Turner (AFRL/RXLMP) P.D. Nicolaou (UES, Inc.) J.P. Thomas (Universal Technology Corp.)				5d. PROJECT NUMBER 4347	
				5e. TASK NUMBER RG	
				5f. WORK UNIT NUMBER M02R2000	
7. PERFORMING ORGANIZATION NAME(S) AND ADDRESS(ES) Metals Branch (AFRL/RXLMP) Metals, Ceramics, and NDE Division Materials and Manufacturing Directorate Wright-Patterson Air Force Base, OH 45433-7750 Air Force Materiel Command, United States Air Force				8. PERFORMING ORGANIZATION REPORT NUMBER AFRL-RX-WP-TP-2008-4336	
9. SPONSORING/MONITORING AGENCY NAME(S) AND ADDRESS(ES) Air Force Research Laboratory Materials and Manufacturing Directorate Wright-Patterson Air Force Base, OH 45433-7750 Air Force Materiel Command United States Air Force				10. SPONSORING/MONITORING AGENCY ACRONYM(S) AFRL/RXLMP	
				11. SPONSORING/MONITORING AGENCY REPORT NUMBER(S) AFRL-RX-WP-TP-2008-4336	
12. DISTRIBUTION/AVAILABILITY STATEMENT Approved for public release; distribution unlimited.					
13. SUPPLEMENTARY NOTES Journal article submitted to the <i>Journal of Engineering Materials and Technology</i> . PAO Case Number: AFRL/WS 07-1598; Clearance Date: 09 Jul 2007. The U.S. Government is joint author of this work and has the right to use, modify, reproduce, release, perform, display, or disclose the work.					
14. ABSTRACT Mechanism-based models for the evolution of defects during the thermomechanical processing of aerospace titanium- and nickel-base alloys are described. These defects include those comprising microstructural/metal-flow irregularities and those that are damage-related (i.e., cracks and cavities.). The development of undesirable/non-uniform microstructures and cavities during the mill processing of alpha/beta titanium alloys is addressed first. Relatively simple, diffusion-based models of spheroidization and coarsening are applied to quantify the propensity for microstructure non-uniformities. Similarly, first order micromechanical models have been formulated to estimate the effect of local crystallographic texture on non-uniform flow, the generation of triaxial stresses, and cavity growth/closure in alpha/beta titanium alloys with a colony-alpha microstructure. The occurrence of non-uniform grain structures (and so-called ALA, or 'as large as,' grains) in cast, wrought, and powder-metallurgy superalloys are also discussed. A physics-based model to treat the topology of recrystallization and the evolution of ALA grains in such materials is proposed.					
15. SUBJECT TERMS defects, spheroidization, coarsening, cavitation, recrystallization					
16. SECURITY CLASSIFICATION OF:			17. LIMITATION OF ABSTRACT: SAR	18. NUMBER OF PAGES 46	19a. NAME OF RESPONSIBLE PERSON (Monitor) Sheldon L. Semiatin 19b. TELEPHONE NUMBER (Include Area Code) N/A
a. REPORT Unclassified	b. ABSTRACT Unclassified	c. THIS PAGE Unclassified			

Defect Occurrence and Modeling for the Thermomechanical Processing of Aerospace Alloys

S.L. Semiatin^a, P.D. Nicolaou^b, J.P. Thomas^c, and T.J. Turner^a

^a Air Force Research Laboratory, Materials and Manufacturing Directorate, AFRL/MLLM, Wright-Patterson AFB, OH 45433-7817

^b UES, Inc., 4401 Dayton-Xenia Road, Dayton, OH 45432

^c Universal Technology Corp., 1270 N. Fairfield Road, Dayton, OH 45432

ABSTRACT

Mechanism-based models for the evolution of defects during the thermomechanical processing of aerospace titanium- and nickel-base alloys are described. These defects include those comprising microstructural/metal-flow irregularities and those that are damage-related (i.e., cracks and cavities). The development of undesirable/non-uniform microstructures and cavities during the mill processing of alpha/beta titanium alloys is addressed first. Relatively simple, diffusion-based models of spheroidization and coarsening are applied to quantify the propensity for microstructure non-uniformities. Similarly, first-order micromechanical models have been formulated to estimate the effect of local crystallographic texture on non-uniform flow, the generation of triaxial stresses, and cavity growth/closure in alpha/beta titanium alloys with a colony-alpha microstructure. The occurrence of non-uniform grain structures (and so-called ALA, or 'as large as', grains) in cast, wrought, and powder-metallurgy superalloys are also discussed. A physics-based model to treat the topology of recrystallization and the evolution of ALA grains in such materials is proposed.

Keywords: defects, spheroidization, coarsening, cavitation, recrystallization

1 Introduction

The thermomechanical processing of aerospace titanium- and nickel-base alloys poses a number of challenges. Often intended for high-temperature applications, these materials have relatively narrow processing windows in terms of temperature and strain rate and are usually produced via complex, multi-step operations. For two-phase alpha-beta titanium alloys [1], for example, ingots with large columnar grains are subjected to hot working and heat treatment in the high-temperature beta (bcc) phase field to produce a finer recrystallized equiaxed grain structure. The beta phase then decomposes during cooling below the transus temperature (at which $\beta \rightarrow \alpha + \beta$) to form colonies of alpha platelets (slow cooling rates) or a basketweave microstructure (faster rates) within the matrix beta grains. Subsequent hot working and annealing high in the two-phase alpha/beta field is used to breakup and spheroidize the transformed lamellar/basketweave microstructure and thus obtain mill product with a structure comprising fine equiaxed-alpha particles in a matrix of beta.

The thermomechanical processing of nickel-based superalloys also consists of multiple steps [2]. For these materials, ingots having large columnar grains are first subjected to a series of upsetting, drawing, and reheating operations above the solvus temperature (at which second phases such as gamma prime are dissolved) in order to obtain a recrystallized equiaxed gamma-grain microstructure. Secondary hot work and heat treatments below the solvus are then conducted to refine the grain size and control the size and distribution of second phases.

Defects that are developed in titanium- and nickel-base alloys are most readily grouped according to whether their origin is related to melting, primary processing, secondary (part) processing, or final heat treatment. Melt processing of titanium ingots can lead to macrosegregation of oxygen, beta stabilizing elements, etc. that produce undesirable variations in beta transus temperature and hence working temperature when selected relative to the transus [3]. In addition, nitrogen-stabilized hard alpha particles and high-density inclusions may be retained in ingots and lead to substantial property debits in final products [4]. Conversion of alpha/beta titanium ingots to billet can give rise to microstructural, textural, and damage-type defects. These include alpha lamellae which are not fully spheroidized (i.e., retained “spaghetti” alpha), regions of spheroidized alpha particles of similar texture that have evolved from a given prior colony (leading to “microtexture”), macroscopic defects (e.g., surface cracks due to die chill, centerbursts due to the development of secondary tensile stresses and poor workability), and microscopic cavities that have originated at the prior-beta grain boundaries during initial alpha/beta hot working [5, 6].

The *secondary* processing of titanium parts can also result in a variety of defects, many of which are metal flow in nature and driven by improper die design and/or material properties [5]. These include laps (metal folding over itself), flow-through defects (e.g., metal flow past a rib in a closed die without filling it), pipe (e.g., suck-in defects at the end of extrudates), and shear bands. Shear bands can be especially troublesome because they may originate due to numerous factors such as poor die/preform design, die chilling, friction, improper

process parameters (e.g., high strain rates that give rise to substantial deformation heating), and material characteristics (e.g., large degrees of flow softening). Part processing may also give rise to defect generation during final heat treatment. For instance, the development of non-uniform texture throughout a titanium part during deformation processing can produce non-uniform beta grain size during final beta annealing due to the interaction of grain growth and texture [7].

A number of the defects found in wrought titanium alloys also can occur in wrought nickel-base superalloys. However, there are also some which are specific to superalloys such as microsegregation, ALA ('as large as') grains, abnormal grains, and thermal cracking [8]. Microsegregation results from alloying element partitioning during solidification and the sluggish kinetics of the homogenization of a number of alloying elements utilized in superalloys to optimize service properties. Grain-size non-uniformities may result from partial recrystallization (ALA grains) or the rapid, preferential growth of a small subset of so-called 'abnormal' grains during supersolvus heat treatment. Last, gross cracking may occur during heating which is too rapid (e.g., ingot/billet reheating prior to hot working) or quenching of thick-section parts following final solution treatment. In both cases, the development of temperatures gradients/thermal stresses act in concert with limited ductility to cause fracture [9].

The great breadth of defects that can be developed in aerospace alloys precludes an extensive treatment of each in the present paper. Thus, the objective of the present work is to provide an overview of several relatively

straightforward, physics-based approaches for analyzing defect generation and illustrate the application of each with an actual production-type problem. The methods to be discussed comprise the bulk-diffusion analysis of the evolution of microstructural defects in titanium alloys, plasticity analyses for cavitation during hot working of textured titanium alloys, and a mesoscale model for describing the non-uniformity of recrystallization during the hot working and heat treatment of superalloys.

2 Microstructural Defects in Alpha/Beta Titanium Alloys

The breakdown of colony (or basketweave) alpha to obtain a fine, equiaxed-alpha microstructure (Figure 1)[†] during primary processing of alpha/beta titanium alloys in the two-phase phase field is controlled by a number metallurgical processes. Each of these processes has an effect on the final alpha particle size and morphology and thus on final strength and fatigue resistance, among other properties. First, preheating prior to hot working leads to coarsening of the alpha platelets; i.e., their thickness increases and length decreases (Figure 2a). Spheroidization *during* subsequent deformation occurs by shearing-type or boundary splitting mechanisms [10]. For this reason, prior static coarsening of the alpha platelets results in substantial and undesirable increases in the strains required for dynamic spheroidization [11]. These strains are typically in excess of those that can be imposed during industrial processes used to fabricate mill products in sizes required for secondary processes such as part forging. Hence, the completion of spheroidization must be accomplished during static, post-

[†] In backscattered-electron (BSE) images taken in a scanning-electron microscope (SEM), the alpha phase is dark, and the beta (or martensitic alpha) phase is white (or gray).

deformation heat treatment (Figure 2b). Static spheroidization occurs by boundary splitting and, to a larger degree, on termination migration [12, 13]. Finally, if the time for completion of the majority of the static spheroidization is exceeded, measurable static coarsening of the equiaxed alpha particles can occur (Figure 2c). As with other metallic materials, static coarsening leads to the growth of large alpha particles and the dissolution of small particles.

2.1 Diffusion Analyses of Microstructure Evolution. Each of the various *static* heat-treatment processes that control microstructure evolution during the breakdown of the colony-alpha morphology in alpha/beta titanium alloys (i.e., coarsening of alpha platelets, spheroidization via termination migration, and coarsening of a spheroidized microstructure) is driven by a reduction in overall alpha/beta interface energy. Furthermore, it has been found that the controlling mechanism by which surface area/energy is reduced is the bulk diffusion of solutes through the beta matrix [14, 15]. In particular, solutes diffuse from regions of high chemical potential/concentration to regions of lower chemical potential/concentration. For the simplest case in which the two phases are ideal, terminal solid solutions, the Gibbs-Thompson equation gives the solute concentration of the matrix ($C_{\beta}(R)$) next to a precipitate (referred to as α) with principal radii of curvature equal to R_1 and R_2 , viz.,

$$C_{\beta}(R)/C_{\beta}(R=\infty) = 1 + (\gamma_{\alpha\beta}\Omega/k_B T) \left(\frac{1}{R_1} + \frac{1}{R_2} \right), \quad (1)$$

in which, $C_\beta(R = \infty)$ denotes the composition next to a flat precipitate (zero curvature), $\gamma_{\alpha\beta}$ is the alpha/beta interface energy, Ω is the atomic volume, k_B is Boltzmann's constant, and T is the absolute temperature.

The application of Equation (1) is simplest for the spheroidization of a lamellar platelet (assumed to have a pancake shape) via termination migration [14]. In such an instance, solute is transferred from the periphery to the flat (plan) surfaces of each (assumed non-interacting) precipitate. As suggested by Courtney and Malzahn Kampe for a similar 2D problem [16], a relatively simple application of Fick's Law to solute diffusion at the beginning and intermediate points of the process can provide reasonable estimates of the spheroidization time. For example, in the beginning of the diffusional process during which the plan surfaces are still relatively flat, the concentration *difference* between the edges and plan surfaces is as follows:

$$[C_\beta (R=\infty)](\gamma_{\alpha\beta}\Omega/k_B T) \left(\frac{2}{t} + \frac{1}{\frac{w}{2} + \frac{t}{4}} \right). \quad (2)$$

Here, t , w are the platelet thickness and diameter, respectively. Geometrical considerations provide estimates of the diffusion distance (and hence concentration gradient) and the area through which the solute flux passes.

Semiatin, *et al.* [14] extended the Courtney and Malzahn Kampe spheroidization analysis to a pancake geometry and modified it to account for the fact that the alpha and beta phases in titanium alloys are not terminal solid solutions. The final result for the spheroidization time, τ_{vd} , was the following:

$$\frac{\tau_{vd}}{\tau'} = \frac{\eta^3 - [0.328\eta^{7/3} (1 + \sqrt{1 - 0.763\eta^{-4/3}})^2]}{4 \left[\frac{2(1+\eta)}{3(0.5 - 0.572\eta^{-1/3})} + \frac{0.5\eta^{1/3} + 0.665\eta^{2/3}}{3(0.143 + 0.934\eta^{-1/3})} \right]} \quad (3a)$$

in which

$$\eta \equiv (w/t) + 0.5 \quad (3b)$$

$$\tau' \equiv t^3 RT / D_\beta C_F \gamma_{\alpha\beta} V_M \quad (3c)$$

$$C_F \equiv \text{Composition Factor} = \frac{C_\beta(1-C_\beta)}{(C_\alpha - C_\beta)^2 [1 + \partial \ln r / \partial \ln C_\beta]} \quad (3d)$$

In Equations (3), R is the gas constant, D_β is the diffusivity of the rate limiting solute in beta titanium, V_M is the molar volume, and C_β ($=C_\beta(R = \infty)$) and C_α are the equilibrium solute concentrations (expressed as atomic fractions) of the rate-limiting solute in the beta and alpha phases, respectively.

The other two diffusion problems mentioned above are more complex. For platelet coarsening, solute is transferred from the edges of a given platelet to its own plan surfaces or to those of adjacent precipitates. The added geometric complexity relative to that for the analysis of spheroidization of an individual platelet is presently under investigation. For static coarsening of a distribution of spherical precipitates, a modified Lifshitz-Slyosov-Wagner (MLSW) analysis [17, 18] has been found to describe kinetics for alpha/beta titanium alloys such as Ti-6Al-4V [15].

2.2 Validation of Static Spheroidization Model. The validity of Equation (3) to quantify the spheroidization behavior and persistence of remnant lamellae was established using observations for Ti-6Al-4V heat treated at 955°C (Figure

2b). At this temperature, the shapes of the lamellae that existed after the completion of boundary splitting (time ≈ 1 h) approximated the idealized pancake geometry assumed in the diffusion model. For Ti-6Al-4V, the diffusion of vanadium through the beta matrix is rate-limiting (in comparison to the diffusion of aluminum).

Model predictions of τ_{vd}/τ' and hence τ_{vd} for spheroidization of the remnant lamellae are given in Table I. The predicted values for the spheroidization time for the pancake-shape geometry ranged from approximately 5 to 15 hours for 5 of the 7 platelets; the other two lamellae were predicted to require times of the order of 30 hours. These values of spheroidization time compare well with the measured time of 12-14 hours to achieve approximately 90 volume pct. of spheroidized microstructure, as defined by alpha particles with an aspect ratio of less than 2:1 [12, 14]. Thus, it is not surprising that a small volume fraction of modest aspect-ratio, partially-spheroidized lamellae would remain after 14 hours (Figure 2b).

3 Plasticity Analyses for Cavitation in Alpha/Beta Titanium Alloys

Internal cavitation represents a second major class of defects in alpha/beta titanium alloys. The control of cavitation is very important because such damage may lead to poor service properties as well as premature failure.

Cavitation during hot working and superplastic forming usually occurs via nucleation, growth, and coalescence processes. Nucleation represents perhaps the most difficult problem to model, and, depending on the mechanism by which it occurs, different approaches have been proposed. For *particle-containing*

materials, such as aluminum and nickel-base alloys, several techniques have been formulated to predict the critical particle size above which cavity nucleation is likely to occur at a given strain rate due to the inability to relax local stress concentrations via diffusion [19-21]. In titanium alloys, which typically do not contain second-phase particles, cavitation is most common during the breakdown hot working of the colony-alpha microstructure (Figure 3). In such cases, an alternate analysis, assuming nucleation due to slip intersections with and/or vacancy coalescence at the prior-beta grain boundaries followed by initial cavity growth under constrained-plasticity conditions, has been proposed [22].

Following nucleation, cavity growth usually occurs via a general-plasticity-controlled mechanism. For *uniaxial-tension* conditions, growth of an *isolated* cavity is then usually described by the following relation [23]:

$$\frac{dr}{d\varepsilon} = \frac{\eta}{3} r , \quad (4)$$

in which r denotes the particle radius as a function of imposed strain ε , and η is the cavity-growth parameter.

In the subsections that follow, several analyses for the growth (*and shrinkage*) of cavities in a typical alpha/beta titanium alloy (Ti-6Al-4V) with a colony-alpha microstructure are summarized.

3.1 Analysis for the Average Cavity Size. The sizes of the cavities that develop during hot working are frequently affected by coalescence with adjacent cavities as well as continuous-nucleation phenomena that occur as deformation proceeds. To quantify these phenomena, Nicolaou and Semiatin [24, 25] conducted a number of mesoscale simulations of cavitation during uniaxial

tension and found that the dependence of the *average* cavity radius \bar{r} on true axial strain ε could be fit by an expression of the following form:

$$\frac{d\bar{r}}{d\varepsilon} = \eta\bar{r}(H + C_v) \quad (5)$$

in which C_v denotes the cavity volume fraction, and H is a constant that depends on the cavity-nucleation conditions. For the case of an initial cavity array for which growth and coalescence occur with no further nucleation, it was found that $H = 1/3$. On the other hand, if cavity nucleation occurs continuously in addition to growth and coalescence, the value of H was shown to decrease to 0.2.

Two modifications to Equation (5) are required to gage the evolution of the average cavity size under complex stress conditions [26]. First, the axial strain ε is replaced by the effective strain $\bar{\varepsilon}$. Second, the cavity-growth parameter for uniaxial tension (η) is replaced by a cavity-growth parameter η^{ts} which is a function of stress triaxiality, or the ratio of the mean stress σ_M to the effective stress $\bar{\sigma}$. Using hot torsion and notched tension tests, Nicolaou, et al. [27-29] determined the ratio of η^{ts}/η . These results were bounded by those from the theoretical analysis of Rice and Tracey [30] for cavity growth under cold-working conditions and the semi-empirical relation derived by Pilling and Ridley [31] for superplastic forming (Figure 4).

The approach developed by Nicolaou and Semiatin [26] to predict the average cavity size developed under complex stress conditions was validated using conventional hot pancake forging of Ti-6Al-4V. During such a forging operation, barreling gives rise to secondary tensile stresses (and thus cavitation)

whose magnitude decreases with distance from the free surface (Figure 5a). Thus, *continuum* finite-element-method (FEM) predictions of the local stress state (Figure 5a), a critical damage factor for cavity nucleation, and values of η^{ts} were combined with Equation (5) to predict the variation of the average cavity size with distance from the free surface. The predictions showed good agreement with measurements (Figure 5b).

3.2 Micromechanical Analysis for the Size of the Largest Cavities.

The classical plasticity-controlled cavity-growth analysis is incapable of predicting the size of the *largest* cavities that are developed during hot working of highly-anisotropic materials such as titanium alloys. In such cases, the dependence of flow properties on crystallographic orientation must be taken into account. To this end, Bieler, et al. [32] and Nicolaou, et al. [26] developed an approximate micromechanical analysis for the stress state and strain partitioning between adjacent “hard” and “soft” colonies in alpha/beta titanium alloys, i.e., those colonies with either large or small Taylor factors, M_h or M_s . One of the basic assumptions of the model was that the cavity formed at the boundary between the hard and soft colonies was small relative to the grain size and hence had little influence on the stresses and strains that would be developed in the absence of the cavity.

For the case of a complex macroscopic stress state, such as would be imposed during metalworking, the micromechanical analysis comprised yield criteria for the hard and soft colonies, equilibrium conditions, and a self-consistent estimate of the strain partitioning between the hard and soft colonies.

The yield criteria in terms of the axial (σ_z), radial (σ_r), and hoop (σ_θ) stress components were the following:

$$\bar{\sigma}_h = \frac{1}{\sqrt{2}} \{ (\sigma_{\theta_h} - \sigma_{z_h})^2 + (\sigma_{z_h} - \sigma_{r_h})^2 + (\sigma_{r_h} - \sigma_{\theta_h})^2 \}^{1/2} \quad (6a)$$

$$\bar{\sigma}_s = \frac{1}{\sqrt{2}} \{ (\sigma_{\theta_s} - \sigma_{z_s})^2 + (\sigma_{z_s} - \sigma_{r_s})^2 + (\sigma_{r_s} - \sigma_{\theta_s})^2 \}^{1/2} \quad (6b)$$

in which the subscripts h and s refer to the hard and soft colonies, and $\bar{\sigma}_s$ and $\bar{\sigma}_h$ denote the flow stress of the soft and hard colonies, respectively.

Cavities were assumed to open on colony/grain boundaries perpendicular to the hoop direction. In such cases, the macroscopic axial (σ_z^{mac}) and radial (σ_r^{mac}) stresses determined from FEM analysis were each assumed to be a rule-of-mixtures average of the corresponding stress components in the hard and soft colonies, thus satisfying the equilibrium considerations, i.e.,

$$\sigma_z^{\text{mac}} = f_h \sigma_{z_h} + (1 - f_h) \sigma_{z_s} \quad (7a)$$

$$\sigma_r^{\text{mac}} = f_h \sigma_{r_h} + (1 - f_h) \sigma_{r_s} \quad (7b)$$

in which f_h denotes the volume fraction of hard colonies. Furthermore, it was assumed that the hoop stress was the same in the soft and hard colonies and was equal to the macroscopic (FEM) stress $\sigma_\theta^{\text{mac}}$, i.e.,

$$\sigma_\theta^{\text{mac}} = \sigma_{\theta_h} = \sigma_{\theta_s} \quad (7c)$$

If the flow stresses of the hard ($\bar{\sigma}_h$) and the soft ($\bar{\sigma}_s$) colonies are known, the axial and radial stresses (and hence stress triaxiality) in each colony can be

determined by solving Equations (6) and (7). Because flow stress is rate sensitive at hot working temperatures, $\bar{\sigma}_s$, $\bar{\sigma}_h$, and the corresponding strain rates were determined by applying a self-consistent model [33]. In this approach, the flow stress of the aggregate $\bar{\sigma}^{mac}$ is given by the following equation:

$$\bar{\sigma}^{mac} = f_h \bar{\sigma}_h + (1 - f_h) \bar{\sigma}_s \quad (8)$$

Assuming that the flow stress is strain rate and strain sensitive, Equation (8) can then be rewritten as

$$\bar{\sigma}^{mac} = f_h k_h (\dot{\bar{\epsilon}}_h)^m (\bar{\epsilon}_h)^n + (1 - f_h) k_s (\dot{\bar{\epsilon}}_s)^m (\bar{\epsilon}_s)^n \quad (9)$$

in which k_h , k_s are the strength coefficients of the hard/soft colonies, which depend only on the Taylor factors M_h/M_s ; $\bar{\epsilon}$, $\dot{\bar{\epsilon}}$ denote the effective strain and strain rate, respectively; and m and n are the strain rate sensitivity index and the strain exponent. Using the self-consistent model, the values of strain rates (and therefore strains) in the hard and soft colonies can then be determined for specific values of k_h and k_s .

For the same hot pancake forging example discussed in Section 3.1, the micromechanical model was used to predict the stress triaxiality and the size of the cavities between adjacent hard and soft colonies, assuming $f_h = 0.6$ (Figure 6). Model predictions of the size of the largest cavities showed good agreement with observations for $M_h/M_s \sim 2$, or values typical of the actual texture [32].

Several of the important aspects of the micromechanical model for the size of the largest cavities developed during hot working of titanium have been validated by detailed crystal-plasticity FEM (CPFEM) calculations. For example, CPFEM [34] has shown that the strain partitioning between hard and soft

colonies is well replicated well by the self-consistent method of Semiatin, *et al.* [33]. Similarly, the stress triaxiality in the soft colony estimated by the simple equilibrium approach shows reasonable agreement with CPFEM results. For example, CPFEM has indicated that the triaxiality in the softer and harder colonies (near the hard-soft colony interface) is approximately 1.0 or 0.05, respectively, for $M_H/M_S = 2.5$, in reasonable agreement with the equilibrium calculations (Figure 6a).

3.3 Cavity-Shrinkage Analysis. Cavities developed during the hot working of anisotropic materials such as alpha/beta titanium alloys may be decreased in size or closed by changes in strain path which give rise to stress triaxiality that is *compressive* in nature. For instance, cavity shrinkage for Ti-6Al-4V subjected to forward torsion followed by reversed torsion or uniaxial compression is illustrated in Figure 7.

An analysis to describe cavity-shrinkage kinetics has been recently developed and validated by Nicolaou and Semiatin [35, 36]. In their approach, the stresses developed within the soft colony/grain (during the strain-path change which gives rise to compressive triaxiality) are estimated in the same manner as in the cavity-growth analysis described in Section 3.2. To estimate the strain-rate components and thus the densification rate ($\dot{\epsilon}_{11} + \dot{\epsilon}_{22} + \dot{\epsilon}_{33}$), the stresses are then inserted into a hybrid model for the consolidation of porous media [37], i.e.,

$$\dot{\epsilon}_{ij} = \left(\frac{K(D)\phi^{2\frac{1}{n}}}{\bar{\sigma}} \right) \left[(1+\nu)\sigma'_{ij} + (1-2\nu)\sigma_m\delta_{ij} \right] \quad (10)$$

in which $\dot{\varepsilon}_{ij}$ denotes the strain rate tensor, σ'_{ij} is the deviatoric stress tensor, σ_M the mean stress, $\bar{\sigma}$ is the effective stress, ν is the Poisson's ratio of the porous body; and ϕ is the stress intensification factor. The function $K(D)$ is associated with the relative density D ; it is commonly assumed to be equal to D for relative densities greater than 90 pct. of full density.

Cavity-shrinkage predictions from the analysis Nicolaou and Semiatin [35, 36] showed good agreement with observations (e.g., the results in Figure 8 for compression following torsion). In particular, the analysis correctly quantified the more rapid closure kinetics during compression compared to reversed torsion (each following forward torsion). Such a result was explained on the basis of the higher levels of compressive stress triaxiality in compression and the orientation of cavities in torsion relative to the applied stresses, among other factors.

4 Mesoscale Model for Recrystallization of Superalloys

Grain size/shape irregularities comprise another major class of defects found in aerospace alloys and are of special concern for iron- and nickel-base superalloys. The prediction of such defects requires models that treat deformation, recrystallization, and grain-growth during thermomechanical processing. A number of techniques have been developed to describe these phenomena. For example, the cellular-automata (CA) approach can be used to simulate microstructure evolution on a relatively small scale, but cannot be applied at every node of an FEM mesh for a finite-size billet/workpiece due to computation limitations. By contrast, simple, phenomenological techniques (such as that based on the Avrami formulation) do not have this drawback, but typically

lack the sophistication required to treat complex problems involving strain rate and temperature transients. Hence, an intermediate (meso-) scale model for microstructure evolution that is mechanism based (as in the CA technique) and computationally efficient (and thus applicable to every node of an FEM mesh) has been developed recently [38-40] and is currently being applied to analyze the occurrence of grain-structure defects in superalloys.

4.1 Formulation of Mesoscale Model. The mesoscale modeling technique comprises two main parts, a geometrical framework and one incorporating driving-force relations that describe the actual evolution of microstructure. To minimize computation requirements, the geometric framework does not represent every grain in an aggregate. Rather, the microstructure description relies on averaging over grain populations that are characterized by similar properties and which are expected to exhibit similar evolution. This requirement leads to the definition of grain families referred to as meso-structure units, or MSUs. To deal with recrystallization, at least two MSUs are necessary: one for the initial grains and another for the recrystallized ones. In the case of multi-hit deformation, such as during cogging of ingots, at least two generations of recrystallized grains are required: one for the grains that appeared during previous hits, which may have grown and then stored some energy again, and those that nucleated during the current or latest deformation step.

The geometric description of microstructure also relies on several assumptions in terms of grain shape (e.g., spherical vs ellipsoidal) and the location of nucleation sites (near existing grain boundaries or inside the initial

grains, as in particle-stimulated nucleation (PSN) of recrystallization). Geometric relations deduced from these assumptions (primarily statistical expectancies of the surface of contact between grains) constrain the geometric variables of MSUs (e.g., grain size, grain density) into a framework that evolves in response to two kinds of inputs: nucleation rates and grain-boundary velocities. From these inputs, the geometric framework allows the autonomous and internally-consistent calculation of the geometric evolution of the various grain populations during their growth-related interactions. A few variables are added to each MSU to quantify dislocation density, sub-boundary density/misorientation, or intrinsic properties such as its Taylor factor.

Driving-force equations are used to evaluate the evolution of the MSU parameters and to deduce from them the required inputs of the geometric framework. The most important of these equations describes the dislocation mean free path (strain hardening), dynamic and metadynamic recovery, sub-boundary generation rate, the kinetics of sub-boundary disorientation, nuclei size, grain boundary mobility and velocity, etc. Details on the mesoscale model can be found in References 39 and 40.

4.2 Mesoscale Model Predictions for ALA Grains. The mesoscale model has been applied to treat the evolution of ALA grains during the breakdown of superalloy ingots with coarse, columnar starting grains [40]. Such materials usually have a grain size of ~5 mm diameter x ~50 mm length and contain ~1000 PSN sites per mm^3 which are clustered in groups of ~10 particles [41].

Two modeling approaches have been used for the ALA problem, one in which the discrete zones of grain-boundary (“necklace”) and intragranular (PSN-recrystallized) grains persist throughout the simulation and the other in which the discrete necklace and PSN zones are converted to a solely wrought-necklace microstructure when the volume fraction of intragranular PSN zones reaches $2/3$ (Figure 9a). It has been found that the evolution of the dynamically-recrystallized volume fraction as a function of strain is essentially identical for the two cases. However, the benefit of the second approach is evident when examining the predicted *size* of the remnant unrecrystallized (ALA) regions (Figure 9b). For the first case, the initial ingot grains seem to disappear suddenly. Hence, this approach in general fails to provide physical insight into the evolution of ALA grains. On the other hand, useful information about the size of the remnants of the initial grains is obtained from the second modeling approach involving the topological conversion. At the moment when the initial ingot grains are converted into wrought-like grains, the curve describing the size of the remnants exhibits a change because the information it provides is no longer based on the initial ingot grains but rather the volume of the new wrought-like remnants. The boundaries of these new grains are inherited primarily from the interfaces of the percolating intragranular zones in which most of the recrystallization has occurred. Thus, they are the true remnants of the initial ingot grains. Following the conversion, the curve describing the size of the remnant unrecrystallized areas exhibits a smooth decrease until recrystallization is complete (Figure 9b).

5 Future Challenges

Physics-based models are invaluable for the design and control of thermomechanical processes for aerospace alloys. However, a number of major challenges remain for the full application of such models to minimize or eliminate defects from finished components. These include the following:

- Micromechanical understanding of phenomena such as cavity nucleation during hot working and abnormal grain growth during final beta heat treatment of titanium alloys.
- Refined CPFEM models which treat the generation, multiplication, and storage of dislocations. Such models are needed for the construction of related physics-based models of dynamic, metadynamic, and static recrystallization of metallic alloys and the defects associated with such metallurgical phenomena.
- Models for residual stress development and distortion, including internal-state-variable constitutive models for complex thermal histories.
- Input data for models, including thermodynamic/kinetic data in both the solid and liquid states (e.g., phase equilibria, mobility/diffusivity data), grain-boundary properties (energy, mobility), and large-strain, high-strain-rate constitutive data and models at cold, warm, and hot-working temperatures.

Acknowledgements- A large portion of this paper was based on work conducted as part of the in-house research activities of the Metals Processing Group of the Air Force Research Laboratory's Materials and Manufacturing Directorate. The support and encouragement of the Laboratory management and the Air Force Office of Scientific Research (Dr. B.P. Conner, program manager) are gratefully acknowledged. Technical discussions with many colleagues, including T.R. Bieler, R.D. Doherty, D.U. Furrer, F. Montheillet, N. Stefansson, and I. Weiss, are also very much appreciated. Two of the authors were supported through Air Force Contracts FA8650-04-D-5235 (PDN) and F33615-03-D-5801 (JPT).

References

- [1] Semiatin, S.L., 1997, "Hot Working of Titanium Alloys - An Overview," in *Advances in the Science and Technology of Titanium Alloy Processing*, I. Weiss, R. Srinivasan, P.J. Bania, D. Eylon, and, S.L. Semiatin, eds., TMS, Warrendale, PA, pp. 3-73.
- [2] Donachie, M.J., and Donachie, S.J., 2002, *Superalloys, A Technical Guide*, ASM International, Materials Park, OH, Chapter 4.
- [3] Wilson, A.F., Jardy, A., Hamel, J., Fox, S.P., and Ablitzer, D., 2004, "Implementation and Utilization of a Mathematical Model to Simulate Vacuum Arc Remelting of Titanium Alloys," in *Ti-2003: Science and Technology*, G. Luetjering and J. Albrecht, eds., Wiley-VCH Verlag GmbH, pp. 149-156.
- [4] Mitchell, A., 1997, "Melting, Casting, and Forging Problems in Titanium Alloys," *JOM*, **49** (6), pp. 40-42.
- [5] Semiatin, S.L., 2003, "Workability in Forging," *Handbook of Workability and Process Design*, G.E. Dieter, H.A. Kuhn, and S.L. Semiatin, eds., ASM International, Materials Park, OH, pp.188-207.
- [6] Woodfield, A.P., Gorman, M.D., Corderman, R.R., Sutliff, J.A., and Yamron, B., 1996, "Effect of Microstructure on Dwell Fatigue Behavior of Ti-6242," in *Titanium '95: Science and Technology*, P.A. Blenkinsop, W.J. Evans, and H.M. Flower, eds., Institute of Metals, London, pp. 1116-1123.
- [7] Ivasishin, O.M., Semiatin, S.L., Markovsky, P.E., Shevchenko, S.V., and Ulshin, S.V., 2002, "Grain Growth and Texture Evolution in Ti-6Al-4V During

Beta Annealing Under Continuous Heating Conditions,” *Materials Science and Engineering A*, **A337**, pp. 88-96.

- [8] Forbes Jones, R.M., and Jackman, L.A., 1999, “The Structural Evolution of Superalloy Ingots during Hot Working,” *JOM*, **51**(1), pp. 27-31.
- [9] Minisandram, R.S., Jackman, L.A., Adaszczik, C.B., and Shivpuri, R., 1997, “Thermal Cracking of Large-Diameter 706 Ingots,” in *Superalloys 718, 625, 706 and Various Derivatives*, E.A. Loria, ed., TMS, Warrendale, PA, pp. 131-139.
- [10] Weiss, I., Welsch, G.E., Froes, F.H., and Eylon, D., 1985, “Mechanisms of Microstructure Refinement in Ti-6Al-4V”, in *Titanium: Science and Technology*, G. Luetjering, U. Zwicker, and W. Bunk, eds., Deutsche Gesellschaft fur Metallkunde e.V., Oberursel, Germany, pp. 1503-1510.
- [11] Shell, E.B., and Semiatin, S.L., 1999, “Effect of Initial Microstructure on Plastic Flow and Dynamic Globularization during Hot Working of Ti-6Al-4V,” *Metall. Mater. Trans. A*, **30A**, pp. 3219-3229.
- [12] Stefansson, N., and Semiatin, S.L., 2003, “Mechanisms of Globularization of Ti-6Al-4V during Static Heat Treatment,” *Metall. Mater. Trans. A*, **34A**, p. 691-698.
- [13] Stefansson, N., Semiatin, S.L., and Eylon, D., 2002, “The Kinetics of Static Globularization of Ti-6Al-4V,” *Metall. Mater. Trans. A*, **33A**, pp. 3527-3534.
- [14] Semiatin, S.L., Stefansson, N., and Doherty, R.D., 2005, “Prediction of the Kinetics of Static Globularization of Ti-6Al-4V,” *Metall. Mater. Trans. A*, **36A**, pp. 1372-1376.

- [15] Semiatin, S.L., Kirby, B.C., and Salishchev, G.A., 2004, "Coarsening Behavior of an Alpha-Beta Titanium Alloy," *Metall. Mater. Trans. A*, **35A**, pp. 2809-2819.
- [16] Courtney, T.H., and Malzahn Kampe, J.C., 1989, "Shape Instabilities of Plate-Like Structures - II. Analysis," *Acta Metall.*, **37**, pp. 1747-1758.
- [17] Voorhees, P.W., and Glicksman, M.E., 1984, "Solution to the Multiparticle Diffusion Problem with Applications to Ostwald Ripening - I.Theory," *Acta Metall.*, **32**, pp. 2001-2011.
- [18] Calderon, H.A., Voorhees, P.W., Murray, J.L., and Kosterz, G., 1994, "Ostwald Ripening in Concentrated Alloys," *Acta Metall. et Mater.*, **42**, pp. 991-1000.
- [19] Needleman, A., and Rice, J.R., 1980, "Plastic Creep Flow Effects in the Diffusive Cavitation of Grain Boundaries," *Acta Metall*, **28**, pp. 1315–1332.
- [20] Stowell, M.J., 1982, "Cavitation in Superplasticity," in *Superplastic Forming of Structural Alloys*, N.E. Paton and C.H. Hamilton, eds., TMS, Warrendale, PA, pp. 321–336.
- [21] Chokshi, A., and Mukherjee, A.K., 1989, "An Analysis of Cavity Nucleation in Superplasticity," *Acta Metall.*, **37**, pp. 3007–3017.
- [22] Ghosh, A.K., Bae, D-H., and Semiatin, S.L., 1999, "Initiation and Early Stages of Cavity Growth during Superplastic and Hot Deformation," *Materials Science Forum*, **304-306**, pp. 609-616.
- [23] Hancock, J.W., 1976, "Creep Cavitation without a Vacancy Flux," *Metal Science*, **10**, pp. 319-325.

- [24] Nicolaou, P.D., and Semiatin, S.L., 1999, "Modeling of Cavity Coalescence during Tensile Deformation," *Acta Mater.*, **47**, pp. 3679-3686.
- [25] Nicolaou, P.D., and Semiatin, S.L., 2000, "An Analysis of the Effect of Continuous Nucleation and Coalescence on Cavitation during Hot Tension Testing," *Acta Mater.*, **48**, pp. 3441-3450.
- [26] Nicolaou, P.D., and Semiatin, S.L., 2005, "An Analysis of Cavity Growth during Open-Die Hot Forging of Ti-6Al-4V," *Metall. Mater. Trans. A*, **36A**, pp. 1567-1574.
- [27] Nicolaou, P.D., and Semiatin, S.L., 2003, "An Experimental and Theoretical Investigation of the Influence of Stress State on Cavitation During Hot Working," *Acta Mater.*, **51**, pp. 613-623.
- [28] Nicolaou, P.D., Goetz, R.L., and Semiatin, S.L., 2004, "Influence of Stress State on Cavitation during Hot Working of Ti-6Al-4V," *Metall. Mater. Trans. A*, **35A**, pp. 655-663.
- [29] Nicolaou, P.D., Miller, J.D., and Semiatin, S.L., 2005, "Cavitation during Hot Torsion Testing of Ti-6Al-4V," *Metall. Mater. Trans. A*, **36A**, pp. 3461-3470.
- [30] Rice, J.R., and Tracey, D.M., 1969, "On the Ductile Enlargement of Voids in Triaxial Stress Fields," *J. Mech. Phys. Solids*, **17**, pp. 201-217.
- [31] Pilling, J., and Ridley, N., 1986, "Effect of Hydrostatic Pressure on Cavitation in Superplastic Aluminum Alloys," *Acta Metall.*, **34**, pp. 669-79.
- [32] Bieler, T.R., Nicolaou, P.D., and Semiatin, S.L., 2005, "An Experimental and Theoretical Investigation of the Effect of Colony Orientation and

Misorientation on Cavitation during Hot Working of Ti-6Al-4V,” *Metall. Mater. Trans. A*, **36A**, pp. 129-140.

[33] Semiatin, S.L., Montheillet, F., Shen, G., and Jonas, J.J., 2002, “Self-Consistent Modeling of the Flow Behavior of Wrought Alpha/Beta Titanium Alloys under Isothermal and Nonisothermal Hot-Working Conditions,” *Metall. Mater. Trans. A*, **33A**, pp. 2719-2727.

[34] Turner, T.J., and Semiatin, S.L., 2004, “A Crystal-Plasticity Model for the Flow Behavior of Two-Phase Alloy Systems,” in *Numiform 2004*, S. Ghosh, J.M. Castro, and J.K. Lee, eds., American Institute of Physics, College Park, MD, pp. 1792-1797.

[35] Nicolaou, P.D., and Semiatin, S.L., 2006, “The Effect of Strain-Path Reversal on Cavitation during Hot Torsion of Ti-6Al-4V,” *Metall. Mater. Trans. A*, **37A**, pp. 3697-3705

[36] Nicolaou, P.D., and Semiatin, S.L., 2007, “Effect of Stress and Strain Path on Cavity Closure during Hot Working of an Alpha/Beta Titanium Alloy,” submitted to *Metall. Mater. Trans. A*.

[37] Dutton, R.E., Shamasundar, S., and Semiatin, S.L., 1995, “Modeling the Hot Consolidation of Ceramic and Metal Powders,” *Metall. Mater. Trans. A*, **26A**, pp. 2041-2052.

[38] Montheillet, F., 1999, “Modeling of the Steady State Regime of Discontinuous Recrystallization,” in *Rex '99*, T. Sakai and H.G. Suzuki, eds., Japan Institute of Metals, Sendai, Japan, pp. 651-658.

- [39] Thomas, J.P., and Semiatin, S.L., 2006, "Mesoscale Modeling of the Recrystallization of Waspaloy and Application to the Simulation of the Ingot-Cogging Process," in *Proceedings, Materials Science and Technology (MS&T) 2006: PROCESSING*, TMS, Warrendale, PA, pp. 609-619.
- [40] Thomas, J.P. Montheillet, F., and Semiatin, S.L., 2007, "A Geometric Framework for Meso-Scale Models of Recrystallization," *Metall. Mater. Trans. A*, **38A**, in press.
- [41] Semiatin, S.L., Weaver, D.S., Fagin, P.N., Glavicic, M.G., Goetz, R.L., Frey, N.D., Kramb, R.C., and Antony, M.M., 2004, "Deformation and Recrystallization Behavior during Hot Working of a Coarse-Grain, Nickel-Base Superalloy Ingot Material," *Metall. Mater. Trans. A*, **35A**, pp. 679-693.

Table I. Geometry of Remnant Alpha Lamellae and Model Predictions of Spheroidization Time at for Ti-6Al-4V at 955°C

Lamella ID	Lamella Diameter, w (μm)	Lamella Thickness, t (μm)	η	τ_{vd}/τ'	τ_{vd} (h)
A	16.4	2.7	6.5	1.39	6.1
B	17.7	3.2	6.1	1.13	7.8
C	18.2	3.6	5.5	0.84	8.6
D	21.8	3.6	6.5	1.39	14.4
E	24.1	2.3	11.1	6.16	15.6
F	27.3	3.6	8.0	2.52	26.1
G	33.2	2.3	15.1	13.6	34.4

Figure Captions

- Figure 1. Microstructures developed in Ti-6Al-4V during primary processing: (a) optical and (inset) SEM BSE micrographs of the colony-alpha microstructure and (b) SEM BSE micrograph of the fine, equiaxed-alpha microstructure.
- Figure 2. Diffusion-controlled processes during the breakdown of the colony-alpha microstructure: (a) static coarsening of alpha plates, (b) static spheroidization of remnant alpha plates following hot working, and (c) classical static coarsening of equiaxed-alpha particles.
- Figure 3. Cavitation developed during hot tension testing of Ti-6Al-4V with a colony-alpha microstructure: (a) optical micrograph, (b) high-magnification SEM BSE image, and (c) electron-backscatter-diffraction (EBSD) inverse-pole figure map indicating presence of hard (basal-oriented) and soft colonies around cavity. The tension axis is vertical in all micrographs.
- Figure 4. Ratio of the cavity-growth parameter under non-uniaxial stress states to that for uniaxial tension (η^{ts}/η) as a function of the stress triaxiality (ratio of the mean stress σ_M to the effective stress $\bar{\sigma}$). The data points (determined using hot torsion and notched tension tests on Ti-6Al-4V) [27-29] are compared to predictions from models of Rice and Tracey [30] and Pilling and Ridley [31].
- Figure 5. Model results for cavitation in a Ti-6Al-4V pancake forging: (a) continuum FEM model predictions of the local stress state at the mid-

height as a function of effective strain and distance from the free surface and (b) comparison of measurements and predictions of the average cavity size after a height reduction of 50 pct. at 815°C. In (b), the sensitivity of the model predictions to input data is illustrated by varying η^{ts} by ± 25 pct relative to its nominal value (i.e., $Q = 0.75, 1,$ or 1.25).

Figure 6. Micromechanical-model predictions for cavitation in Ti-6Al-4V with a colony-alpha microstructure which was hot pancake forged at 815°C: (a) stress triaxiality in adjacent hard and soft colonies at the equatorial free surface as a function of effective strain and the Taylor-factor ratio (M_h/M_s) and (b) cavity size after a 50-pct. reduction as a function of the Taylor-factor ratio and distance from the equatorial free surface. The cavity-size predictions in (b) are compared to measurements (data points).

Figure 7. Micrographs illustrating the effect of strain path on cavitation in samples of Ti-6Al-4V with a colony-alpha microstructure subjected to hot deformation at 815°C and an effective strain rate of 0.04 s^{-1} : (a) forward torsion to a surface effective strain of 0.99, or forward torsion to a surface effective strain of 0.99 followed by (b) reversed torsion to a surface effective strain of 0.25, or (c) uniaxial compression along the prior torsion axis to a height strain of -0.29. The torsion/compression axis is vertical and the radial direction is horizontal in the micrographs.

Figure 8. Model predictions of the reduction in cavity volume fraction as a function of macroscopic effective strain during compression of Ti-6Al-4V with a colony-alpha microstructure following torsion to the indicated surface effective strains. Torsional prestraining and subsequent compression were both conducted at 815°C and an effective strain rate of 0.04 s⁻¹. The predictions are compared to experimental results (data points).

Figure 9. Mesoscale model for simulating the evolution of recrystallization nucleated at grain boundaries and intragranular particles in superalloy ingots with coarse, columnar grains: (a) schematic illustration of the topology of recrystallization and (b) predicted size of the remnant, unrecrystallized (ALA) grains for the cases in which (i) the original topology was retained throughout the simulation (solid line) and (ii) the original topology was converted to a necklace-only one once the intragranular recrystallized regions had percolated throughout the initial ingot grains (broken line). The nucleation rate was 1 nucleus per 100 μm² of boundary and per unit strain, the grain-boundary velocity was 10 μm per unit strain, and the volume of each nucleus was 1000 μm³.

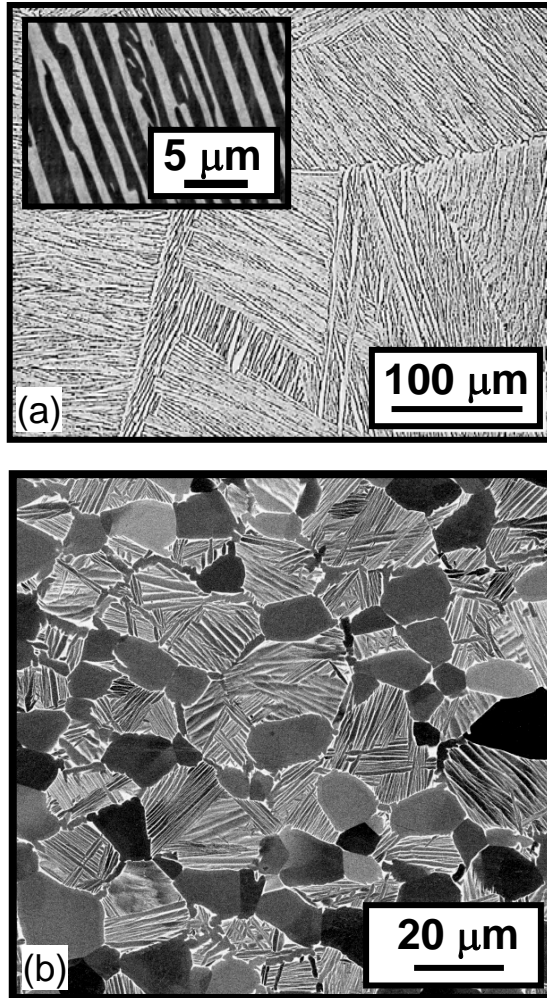


Figure 1. Microstructures developed in Ti-6Al-4V during primary processing: (a) optical and (inset) SEM BSE micrographs of the colony-alpha microstructure and (b) SEM BSE micrograph of the fine, equiaxed-alpha microstructure.

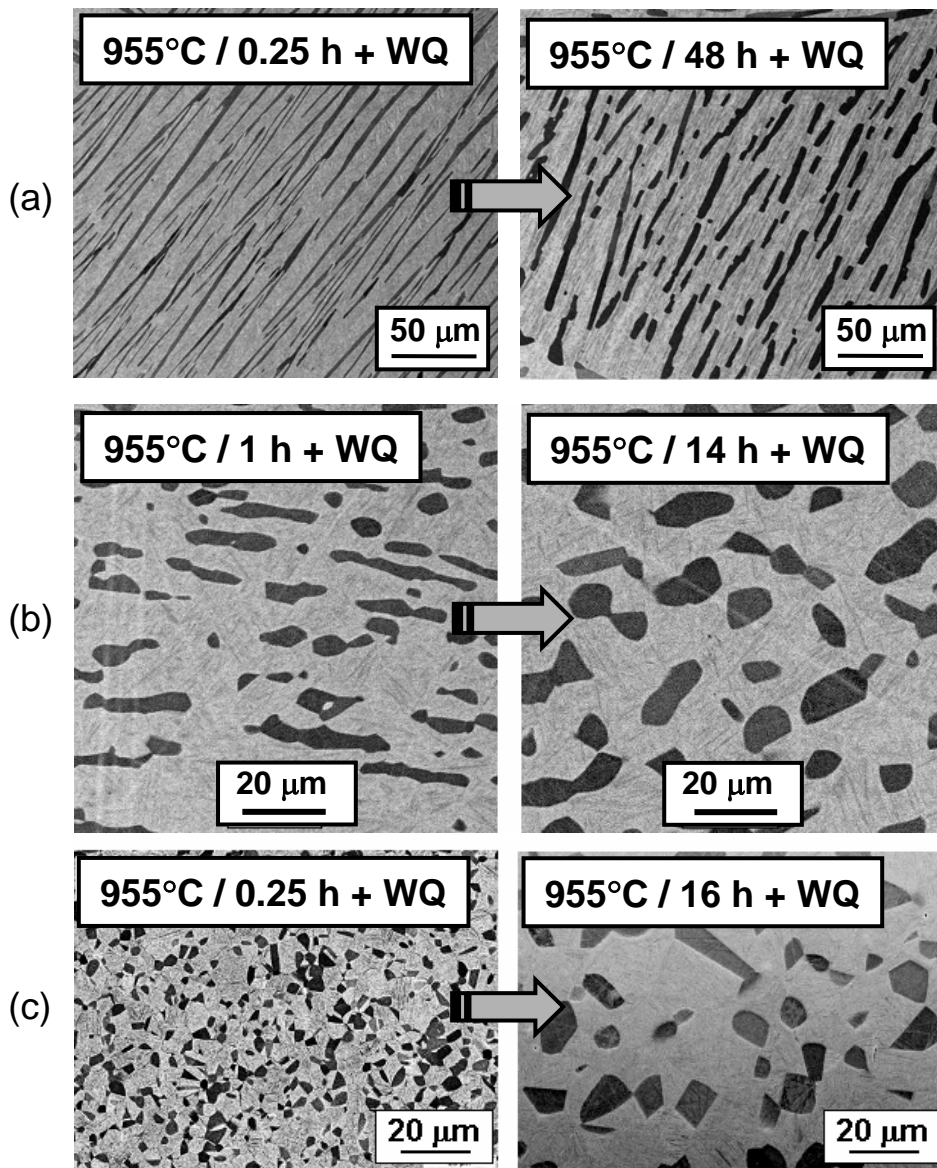


Figure 2. Diffusion-controlled processes during the breakdown of the colony-alpha microstructure: (a) static coarsening of alpha plates, (b) static spheroidization of remnant alpha plates following hot working, and (c) classical static coarsening of equiaxed alpha particles.

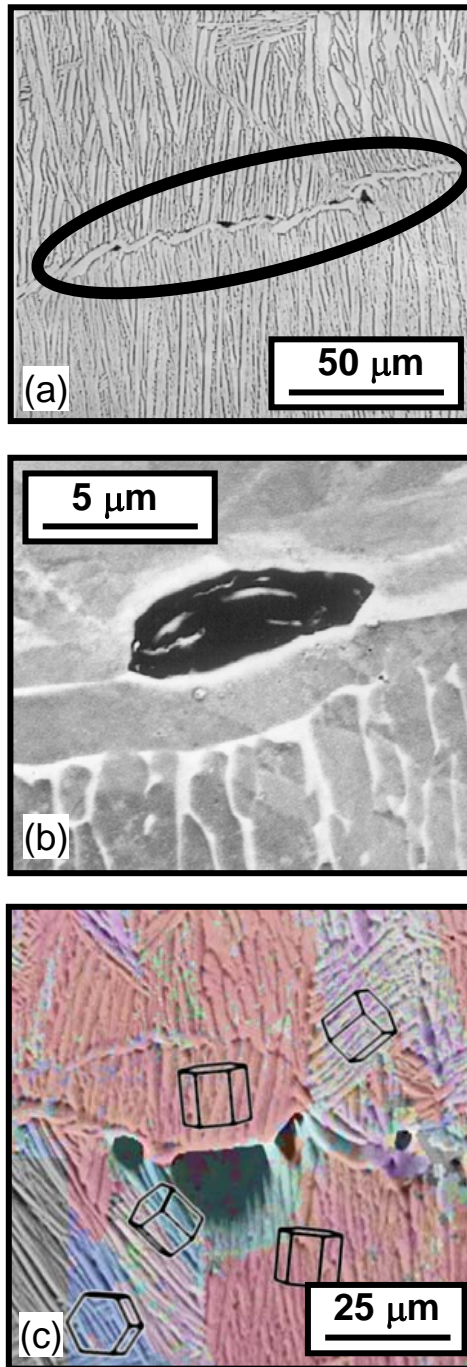


Figure 3. Cavitation developed during hot tension testing of Ti-6Al-4V with a colony-alpha microstructure: (a) optical micrograph, (b) high-magnification SEM BSE image, and (c) electron-backscatter-diffraction (EBSD) inverse-pole figure map indicating presence of hard (basal-oriented) and soft colonies around cavity. The tension axis is vertical in all micrographs.

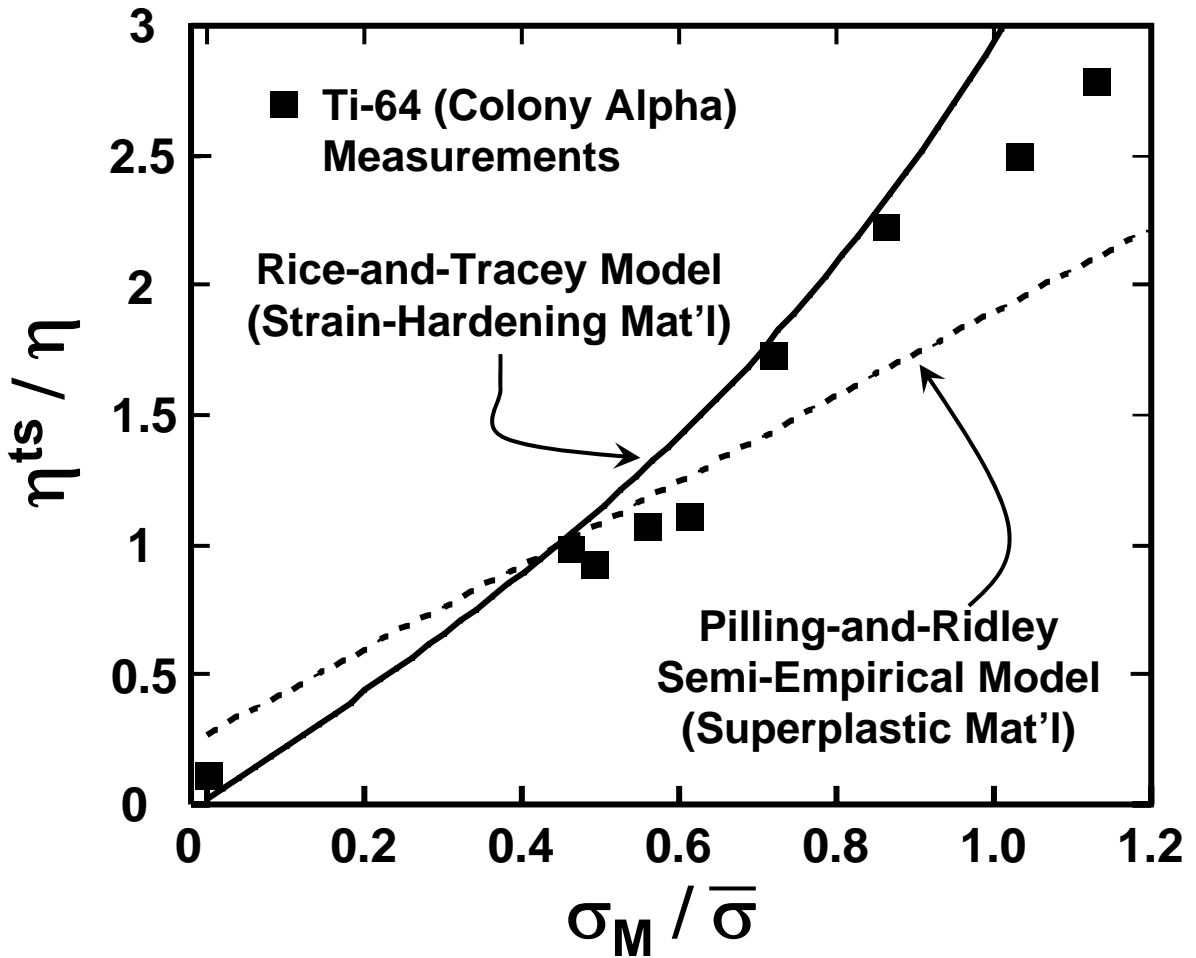


Figure 4. Ratio of the cavity growth parameter under non-uniaxial stress states to that for uniaxial tension (η^{ts}/η) as a function of the stress triaxiality (ratio of the mean stress σ_M to the effective stress $\bar{\sigma}$). The data points (determined using hot torsion and notched tension tests on Ti-6Al-4V) [27-29] are compared to predictions from models of Rice and Tracey [30] and Pilling and Ridley [31].

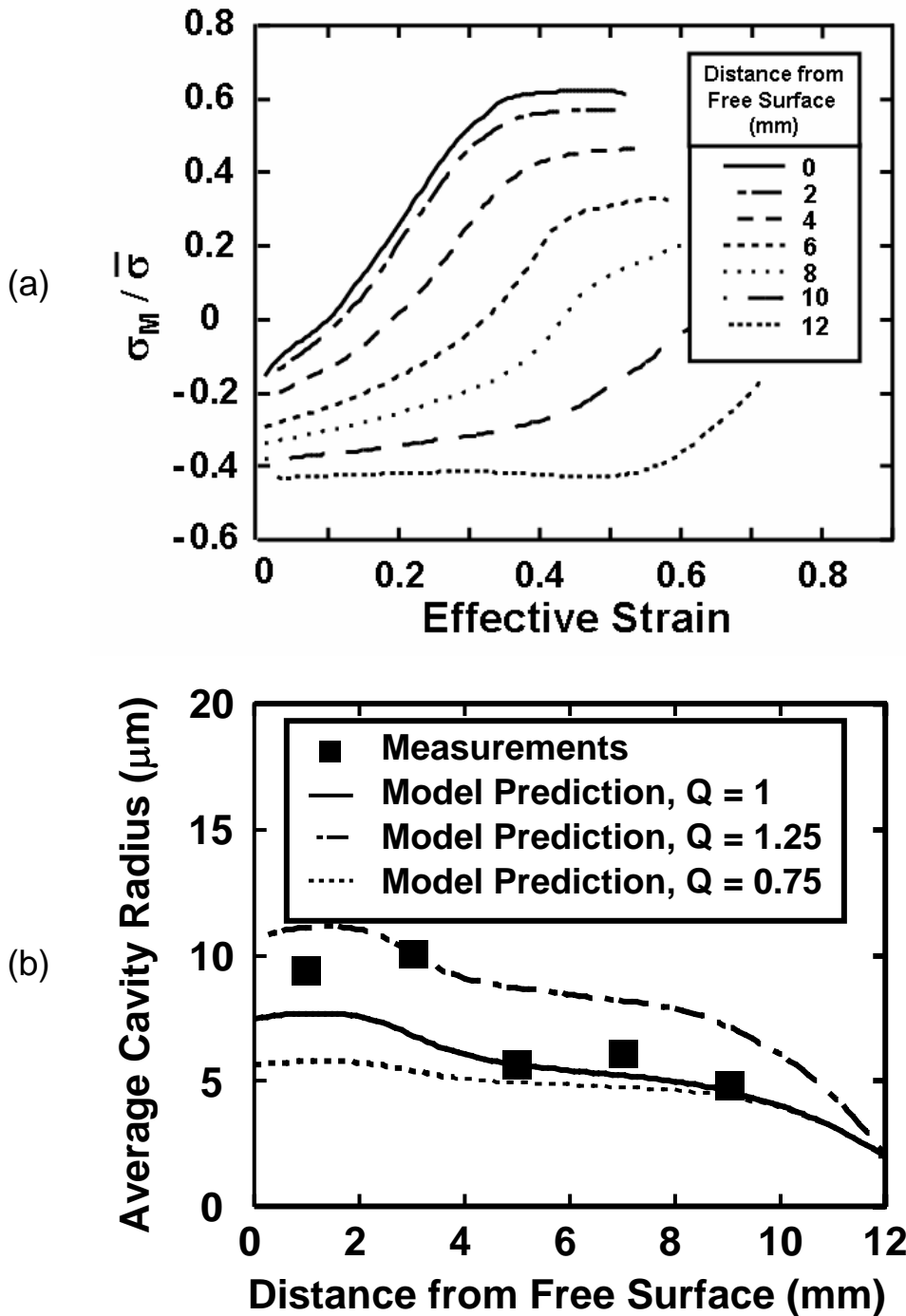


Figure 5. Model results for cavitation in a Ti-6Al-4V pancake forging: (a) continuum FEM model predictions of the local stress state at the mid-height as a function of effective strain and distance from the free surface and (b) comparison of measurements and predictions of the average cavity size after a height reduction of 50 pct. at 815°C. In (b), the sensitivity of the model predictions to input data is illustrated by varying η^{ts} by ± 25 pct relative to its nominal value (i.e., $Q = 0.75$, 1, or 1.25).

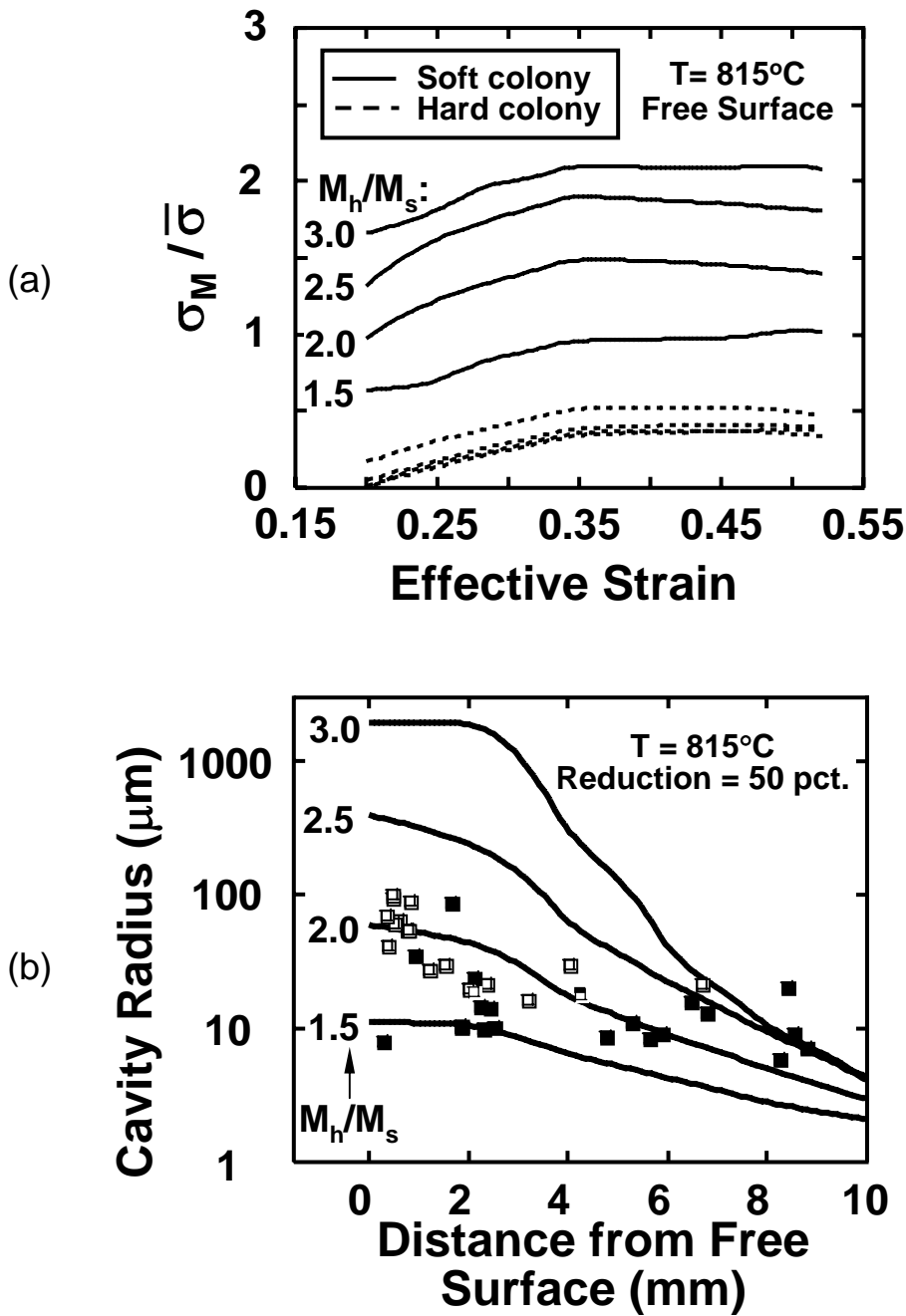


Figure 6. Micromechanical-model predictions for cavitation in Ti-6Al-4V with a colony- α microstructure which was hot pancake forged at 815°C: (a) stress triaxiality in adjacent hard and soft colonies at the equatorial free surface as a function of effective strain and the Taylor-factor ratio (M_h/M_s) and (b) cavity size after a 50-pct. reduction as a function of the Taylor-factor ratio and distance from the equatorial free surface. The cavity-size predictions in (b) are compared to measurements (data points).

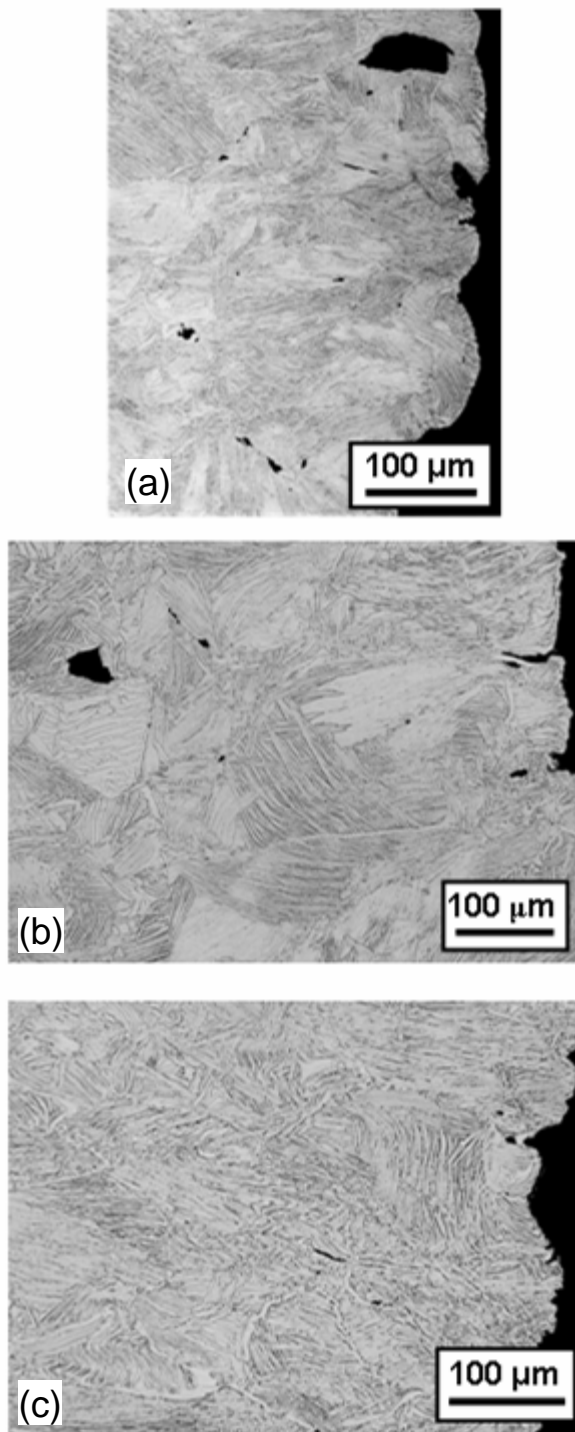


Figure 7. Micrographs illustrating the effect of strain path on cavitation in samples of Ti-6Al-4V with a colony-alpha microstructure subjected to hot deformation at 815°C and an effective strain rate of 0.04 s^{-1} : (a) forward torsion to a surface effective strain of 0.99, or forward torsion to a surface effective strain of 0.99 followed by (b) reversed torsion to a surface effective strain of 0.25, or (c) uniaxial compression along the prior torsion axis to a height strain of -0.29. The torsion/compression axis is vertical and the radial direction is horizontal in the micrographs.

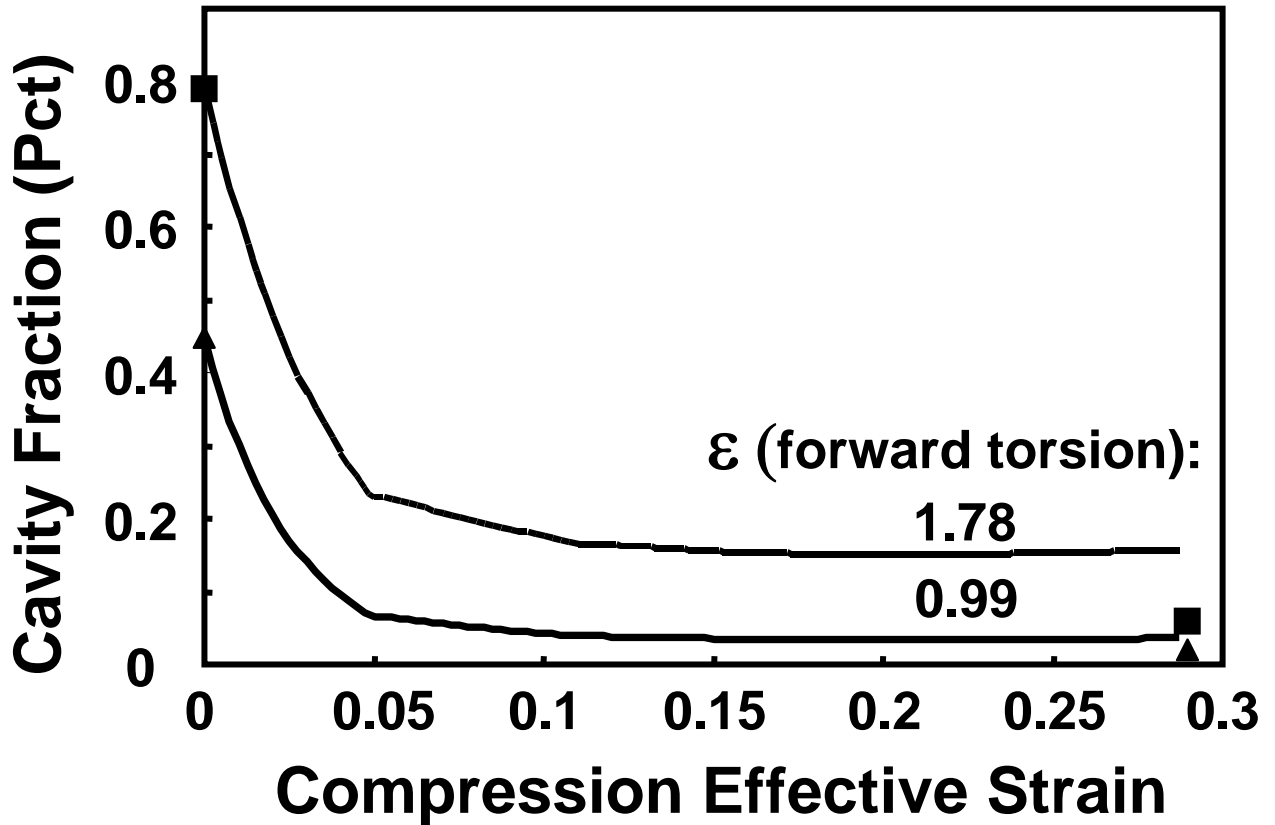
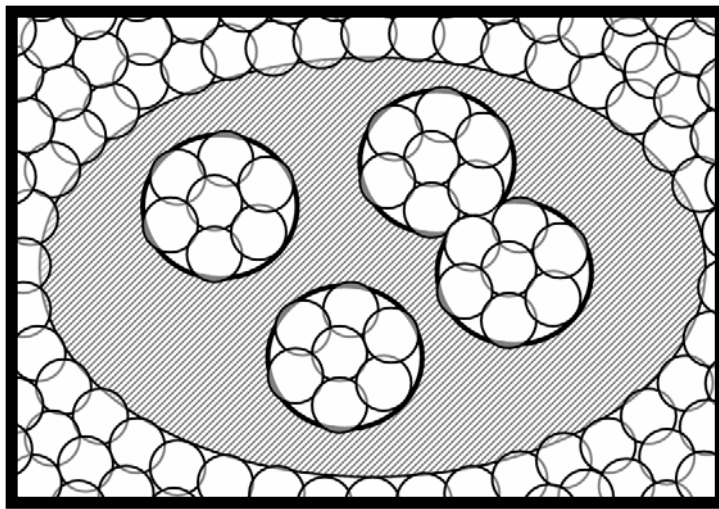


Figure 8. Model predictions of the reduction in cavity volume fraction as a function of macroscopic effective strain during compression of Ti-6Al-4V with a colony-alpha microstructure following torsion to the indicated surface effective strains. Torsional prestraining and subsequent compression were both conducted at 815°C and an effective strain rate of 0.04 s⁻¹. The predictions are compared to experimental results (data points).

(a)



(b)

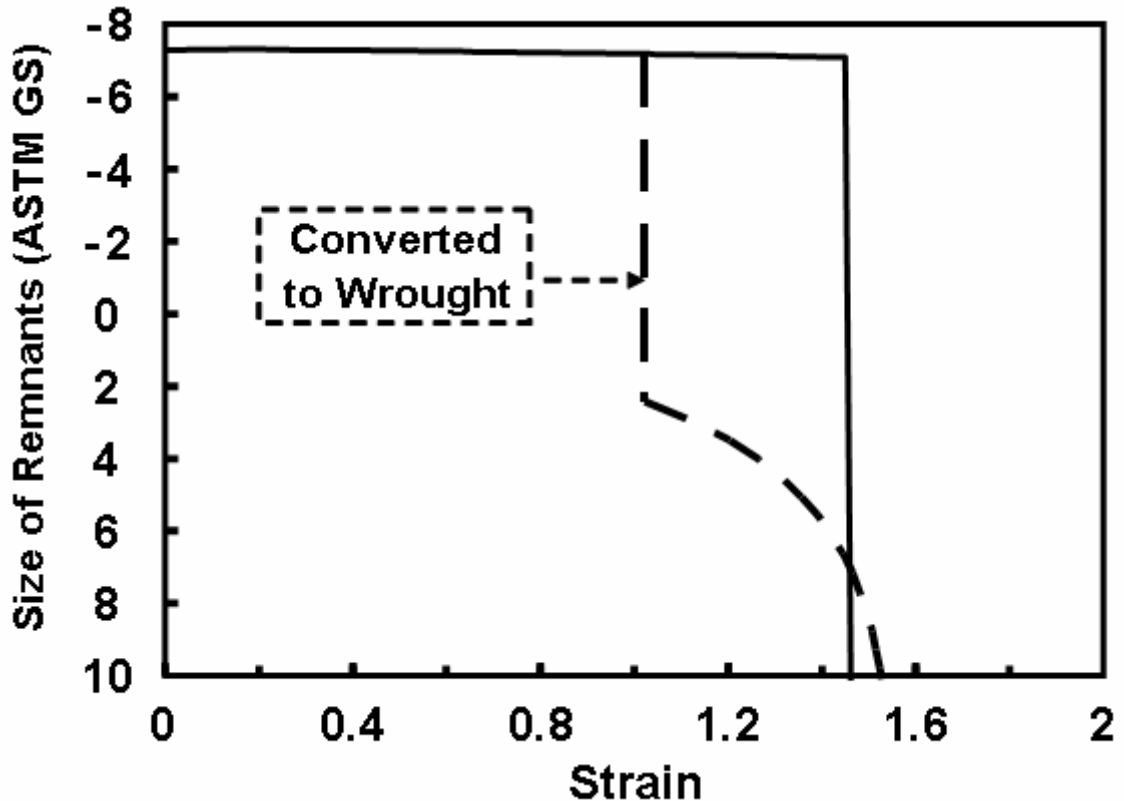


Figure 9. Mesoscale model for simulating the evolution of recrystallization nucleated at grain boundaries and intragranular particles in superalloy ingots with coarse, columnar grains: (a) schematic illustration of the topology of recrystallization and (b) predicted size of the remnant, unrecrystallized (ALA) grains for the cases in which (i) the original topology was retained throughout the simulation (solid line) and (ii) the original topology was converted to a necklace-only one once the intragranular recrystallized regions had percolated throughout the initial ingot grains (broken line). The nucleation rate was 1 nucleus per $100 \mu\text{m}^2$ of boundary and per unit strain, the grain-boundary velocity was $10 \mu\text{m}$ per unit strain, and the volume of each nucleus was $1000 \mu\text{m}^3$.